Fluid shear stress threshold regulates angiogenic sprouting

Peter A. Galie[a,b], Duc-Huy T. Nguyen[c], Colin K. Choi[a], Daniel M. Cohen[a], Paul A. Janmey[b], and Christopher S. Chen[a,c,d,e,1]

Departments of [a]Bioengineering, [b]Physiology, and [c]Chemical and Biomolecular Engineering, University of Pennsylvania, Philadelphia, PA 19104; [d]Department of Biomedical Engineering, Boston University, Boston, MA 02215; and [e]The Wyss Institute for Biologically Inspired Engineering, Harvard University, Boston, MA 02115

Edited by Sheldon Weinbaum, The City College of New York, New York, NY, and approved April 21, 2014 (received for review June 7, 2013)

The density and architecture of capillary beds that form within a tissue depend on many factors, including local metabolic demand and blood flow. Here, using microfluidic control of local fluid mechanics, we show the existence of a previously unappreciated flow-induced shear stress threshold that triggers angiogenic sprouting. Both intraluminal shear stress over the endothelium and transmural flow through the endothelium above 10 dyn/cm^2 triggered endothelial cells to sprout and invade into the underlying matrix, and this threshold is not impacted by the maturation of cell–cell junctions or pressure gradient across the monolayer. Antagonizing VE-cadherin widened cell–cell junctions and reduced the applied shear stress for a given transmural flow rate, but did not affect the shear threshold for sprouting. Furthermore, both transmural and luminal flow induced expression of matrix metalloproteinase 1, and this up-regulation was required for the flow-induced sprouting. Once sprouting was initiated, continuous flow was needed to both sustain sprouting and prevent retraction. To explore the potential ramifications of a shear threshold on the spatial patterning of new sprouts, we used finite-element modeling to predict fluid shear in a variety of geometric settings and then experimentally demonstrated that transmural flow guided preferential sprouting toward paths of draining interstitial fluid flow as might occur to connect capillary beds to venules or lymphatics. In addition, we show that luminal shear increases in local narrowings of vessels to trigger sprouting, perhaps ultimately to normalize shear stress across the vasculature. Together, these studies highlight the role of shear stress in controlling angiogenic sprouting and offer a potential homeostatic mechanism for regulating vascular density.

angiogenesis | force | mechanotransduction | migration | morphogenesis

The density of capillary blood vessels varies widely across different organs and tissues and is determined by the ability of unmet local metabolic needs to trigger angiogenesis. Perhaps most well characterized is the induction of VEGF expression by parenchymal hypoxia, leading to angiogenesis that persists until the hypoxia is relieved by subsequent enhanced tissue perfusion (1). Indeed, significant advances have been made in understanding the mechanisms by which numerous biochemical stimuli induce endothelial sprouting (2). Importantly, excess metabolic demand also triggers enhanced local circulation by relaxation of upstream arterioles (3) and results in increased blood flow to these regions. In addition to enhanced delivery of nutrients, the increased blood flow also increases shear stress on the luminal surface of the endothelium, which in some studies has been shown to induce capillary growth in skeletal muscle (4, 5), whereas others showed shear stress enhances endothelial barrier function and inhibits sprouting (6–9).

Unlike luminal shear, transmural flow, or fluid flow exiting the wall of the vessel, is universally accepted to induce sprouting of endothelial cells into the extracellular matrix, at least in in vitro models (9–11). Transmural flow is directed normal to the surface of cells and thus simultaneously exerts both a pressure stress against the apical surface of the cell and a shear stress concentrated at the cell membrane adjacent to intercellular junctions (12–14). The present study seeks to elucidate the reasons that transmural flow consistently induces sprouting whereas the effects of luminal flow are more controversial, despite both flows exerting shear stress on the endothelium.

Here, we use a series of microfabricated microfluidic devices to demonstrate that a threshold of shear stress exists above which cells will sprout regardless of whether the shear is exerted by transmural or luminal fluid flow. Moreover, we demonstrate how the shear threshold can guide enhanced sprouting at regions of constricted diameter and focus sprouting in the direction of transmural flow. These results underscore the importance of shear stress as a crucial parameter for the initiation of angiogenesis and the regulation of structures within a vasculature bed and highlight the interplay between mechanical, structural, and biochemical signals that cells use to organize and adapt the vasculature to meet its many functional demands.

Results

Both Transmural and Luminal Flow-Induced Sprouting Are Triggered by a Common Threshold of Shear Stress. To test the effect of transmural flow on sprouting, we first seeded cells on a constrained 2-mg/mL collagen gel of known permeability (15) formed as a plug within a flow chamber (Fig. S1 *B*, *i*), allowed them to attach and develop a confluent monolayer over 36 h, and then applied transmural flow to the monolayer. After 24 h of transmural flow resulting in junctional velocities greater than 5 μm/s, we observed copious sprouting of cells into the collagen gel along the monolayer of seeded cells (Fig. 1 *A* and *B*). Quantifying the length of sprouts, it was evident that this effect depended sharply on the junctional velocity (Fig. 1*C*). However, changing the junctional

Significance

A great deal of research has investigated the biochemical factors that regulate angiogenic sprouting, but less is known about the role of fluid shear stress. Some studies have suggested distinct regulation by luminal flow within the vessel vs. transmural flow through its walls. In this paper, we demonstrate the existence of a shear stress threshold that when surpassed, induces angiogenic sprouting regardless of whether the shear is applied by primarily luminal or transmural flow. In addition to identifying matrix metalloproteinase 1 as the relevant downstream effector, we use finite-element modeling to predict spatial distributions of shear stress within 3D geometries that experimentally caused localized patterns of sprouting. Together, these studies demonstrate a means by which fluid flow can guide vasculature architecture.

Author contributions: P.A.G., D.M.C., and P.A.J. designed research; P.A.G. performed research; D.-H.T.N. and C.K.C. contributed new reagents/analytic tools; P.A.G. and C.S.C. analyzed data; and P.A.G. wrote the paper.

The authors declare no conflict of interest.

This article is a PNAS Direct Submission.

[1]To whom correspondence should be addressed. E-mail: chencs@bu.edu.

This article contains supporting information online at www.pnas.org/lookup/suppl/doi:10.1073/pnas.1310842111/-/DCSupplemental.

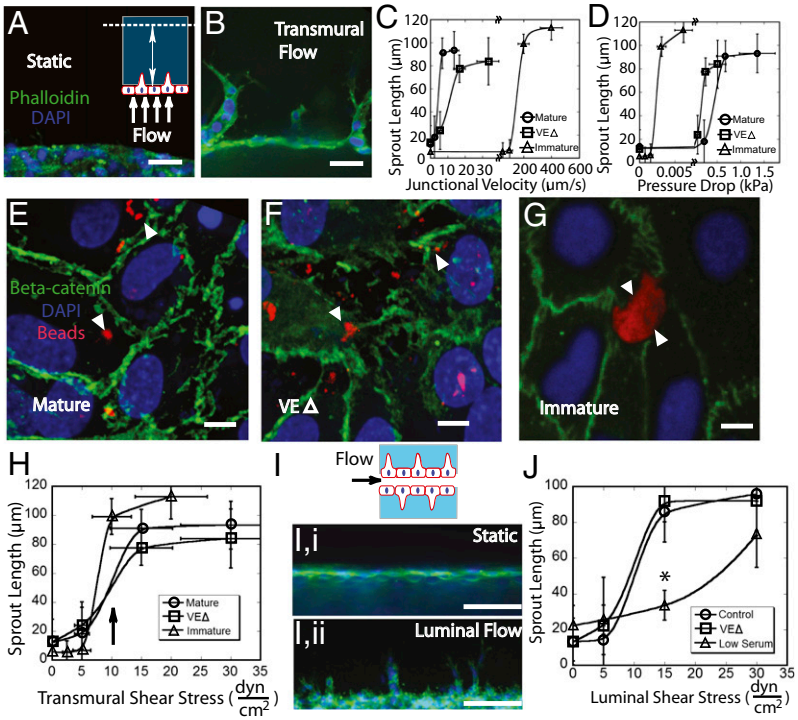

Fig. 1. (*A* and *B*) Schematic and representative image of a mature endothelial cell monolayer plated on the surface of a collagen gel (*A*) and sprouting in response to perfusion with transmural flow (*B*). (Scale bar, 50 μm.) (*C* and *D*) Mean sprout length of mature untreated and VEΔ monolayers and immature monolayers exposed to transmural flow of several junctional velocities (*C*) and pressure drops (*D*). Linear ANOVAs followed by Tukey tests were used to determine that the sprouting responses of control and VEΔ groups were significantly different (*$P < 0.05$). (*E*–*G*) Monolayer of mature untreated (*E*) and VEΔ (*F*) and immature (*G*) conditions. Green, β-catenin; blue, nucleus; red, 1-μm beads. The white arrowheads point to the distributed beads accumulated on the monolayer surface. (Scale bar, 10 μm.) (*H*) Mean sprout length as a function of transmural shear for nontreated mature, VEΔ mature, and immature monolayers. Again, post hoc Tukey tests were conducted to calculate the significant difference in the reduced serum group (*$P < 0.05$). (*I*) Surface of cylindrical channel for static (*I*, *i*) and luminal flow (*I*, *ii*) conditions. Green, F-actin; blue, nucleus. (Scale bar, 100 μm.) (*J*) Mean sprout length as a function of luminal shear for nontreated and VEΔ cells and cells exposed to 0.5% serum.

velocity impacts both the pressure force normal to the luminal face of the endothelial cells and the shear stress on cell–cell junctions.

To distinguish whether the sprouting response was dictated by velocity, pressure, or shear, we modulated junctional integrity to decouple these effects. That is, varying the distance between cells by loosening cell–cell junctions would allow us to reduce applied pressure drop and shear stress for a specified junctional velocity. We used atomic force microscopy (AFM) and transmission electron microscopy (TEM) to determine the precise geometry and spacing of the junctions between cells to estimate the relationship between pressure drop, junctional velocity, and shear stress magnitude at the cell–cell junctions (Figs. S2 and S3). Cells were transduced to express a mutant VE-cadherin lacking its β-catenin binding domain (VEΔ). We chose VE-cadherin because of its modulation of vascular permeability and angiogenesis (16) and involvement in fluid shear mechanotransduction (17). We verified the effects of VEΔ by immunofluorescence of monolayers exposed to perfusion with media containing suspended 1-μm beads (Fig. 1 *E*–*G*). Control monolayers exhibited localization of β-catenin to the cell–cell junctions (green), and the fluorescent beads (red) settled throughout the monolayer (Fig. 1*E*), whereas VEΔ-treated monolayers exhibited β-catenin only partially localized to cell–cell junctions with substantial perinuclear staining, and beads again were scattered homogeneously (Fig. 1*F*). Cells treated with VEΔ required a higher junctional velocity to sprout, but a lower applied pressure drop compared with control monolayers (Fig. 1 *C* and *D*). These results suggest that neither pressure drop nor junctional velocity is the universal quantity that determines sprouting. Because direct inhibition of VE-cadherin function could impact other signaling functions such as modulation of VEGF receptor signaling, we also altered junctional geometry by examining flow-induced sprouting from immature monolayers. Here, we applied flow 30 min after cell seeding, rather than waiting 36 h for a mature monolayer to form. The resulting immature monolayers exhibited hydraulic conductivities several orders of magnitude greater than values calculated for the mature monolayers of control and VEΔ-treated cells ($5.91E$-8 and $1.03E$-6 $cm \cdot s^{-1} \cdot cm^{-1}$ H_2O), which are within the range of previous values reported for endothelial monolayers (18). Indeed, for the immature monolayers, beads accumulated in large gaps within the monolayer (Fig. 1*G*). The immature monolayers sprouted in response to substantially higher junctional velocities and lower pressure drops compared with controls (Fig. 1 *C* and *D*), again suggesting that these are not the physical factors transduced by cells to induce sprouting. Instead, replotting our results as a function of shear stress indicated that sprouting occurred at the same shear stress threshold (~ 10 dyn/cm^2) in all three conditions (Fig. 1*H*).

To test whether luminal shear stress had similar or distinct effects on sprouting, we seeded cells in a cylindrical channel within the collagen hydrogel, using a method adapted from Tien and coworkers (19) (Fig. S1 *B*, *ii*). In this configuration, computational modeling verified that flow along the channels resulted in primarily luminal shear with minimal transmural shear (Fig. S4). We again observed a threshold for sprouting similar to that of transmural flow (Fig. 1 *I*, *i* and *ii*). This finding indicates that the location where shear stress was exerted, whether at cell–cell junctions or along the luminal (apical) face of the cell, did not affect the threshold required for sprouting. Moreover, VEΔ-treated monolayers sprouted at the same threshold of luminal shear as untreated,

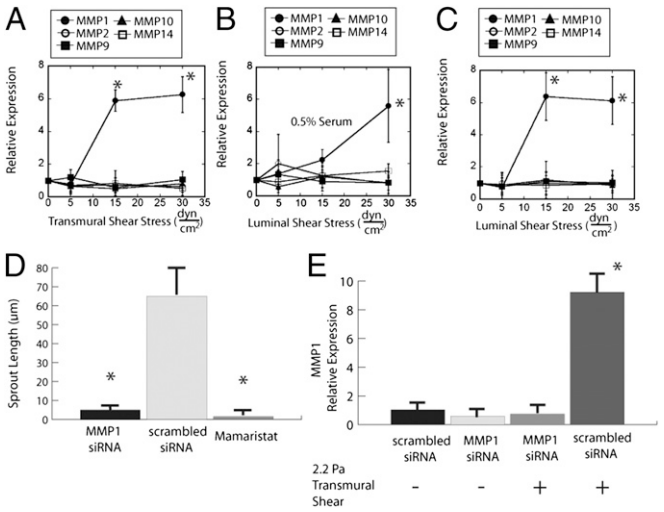

Fig. 2. (*A*) MMP message levels for MMP1, MMP2, MMP9, MMP10, and MMP14 double normalized to GAPDH and static controls in response to transmural shear stress. Two-sample *t* tests were performed for each MMP primer to determine statistical significance between the applied shear and static controls (*P < 0.05). (*B*) MMP message levels for cells exposed to luminal flow and reduced serum (*P < 0.05). (*C*) MMP message levels in response to luminal flow (*P < 0.05). (*D*) Mean sprout length for cells treated with MMP1 DsiRNA, a scrambled DsiRNA control, and Mamaristat. Two-sample *t* tests were calculated to test for a significant change from untreated controls (*P < 0.05). (*E*) Validation of successful knockdown by qRT-PCR. Transmural flow only significantly increases message levels of MMP1 (*P < 0.05).

mature monolayers, confirming our previous conclusion that widening cell–cell junctions suppressed transmural flow-induced sprouting for a given junctional velocity by decreasing shear stress at the cell–cell junctions, not by disrupting the ability of cells to respond to mechanical cues.

The observed shear threshold of ~10 dyn/cm^2 is lower than the physiological shear that occurs in nonsprouting vessels in vivo, suggesting that additional aspects of the in vivo context may increase the threshold for the sprouting response. One possibility is that in vitro culture uses a high level of serum, which contains proangiogenic factors from lysed platelets, whereas in vivo plasma is relatively replete of growth factors. We therefore perfused flow using medium with reduced serum (0.5% vs. 2%) and observed an increase in the threshold of shear above which sprouting occurs (20–30 dyn/cm^2) (Fig. 1*J*). These results suggest that although we have identified a previously unappreciated shear stress threshold for inducing angiogenic sprouting, the value of that threshold may shift, depending on the environmental context.

The Downstream Effector for Flow-Induced Sprouting Is Matrix Metalloproteinase 1. Because luminal flow acts on the apical surface of the endothelial cell whereas transmural flow acts on the cell–cell junctions, it was not clear whether the mechanisms for sprouting in the two settings were shared or distinct. Here, we explored by quantitative (q)RT-PCR whether transmural and luminal flows altered expression of selected members of the matrix metalloproteinase (MMP) family, whose expression is critical in 3D cell migration and sprouting (20). Cells first were exposed to different levels of transmural flow for 24 h in the same configurations detailed in Fig. 1 and lysed for analysis of MMP expression. MMP1 was the only member of the MMP family significantly up-regulated in response to flow (Fig. 2*A*). Importantly, the degree of MMP1 expression was sensitive to the level of applied shear stress such that it increased most dramatically at the same threshold when sprouting became substantial. None of the other measured MMPs changed expression in response to shear stress. Interestingly, in cells exposed to reduced serum, MMP1 up-regulation again mirrored the sprouting response. More luminal shear stress was required to significantly increase MMP1 expression in cells treated with reduced serum (Fig. 2*B*). Luminal shear stress also up-regulated MMP1 only at the established shear threshold of ~10 dyn/cm^2 for 2% serum. (Fig. 2*C*). These results confirmed that not only do both transmural and luminal shear stresses induce sprouting at the same threshold, but also the up-regulation of MMP1 correlated with the sprouting response.

To examine whether the shear stress-induced MMP1 up-regulation was causally required for the sprouting response, we transiently transfected a dicer substrate interference RNA (DsiRNA) targeting MMP1 into endothelial cells and exposed cells to 22 dyn/cm^2 of transmural shear stress. Silencing the MMP1 message blunted the increased sprout length in response to transmural shear. Conversely, a scrambled DsiRNA construct did not have any significant effect on the sprouting response (Fig. 2*D*). Mamaristat, a broad spectrum MMP inhibitor (21), similarly blocked flow-induced sprouting and confirmed that MMP1 is the crucial matrix metalloproteinase for flow-induced sprouting. To validate the knockdown of the DsiRNA, we used qRT-PCR to analyze the expression of MMP1 in response to control and 22 dyn/cm^2 transmural shear stress conditions. Fig. 2*E* indicates that in response to flow, the siRNA knockdown prevents the augmented expression of MMP1, whereas a scrambled construct does not.

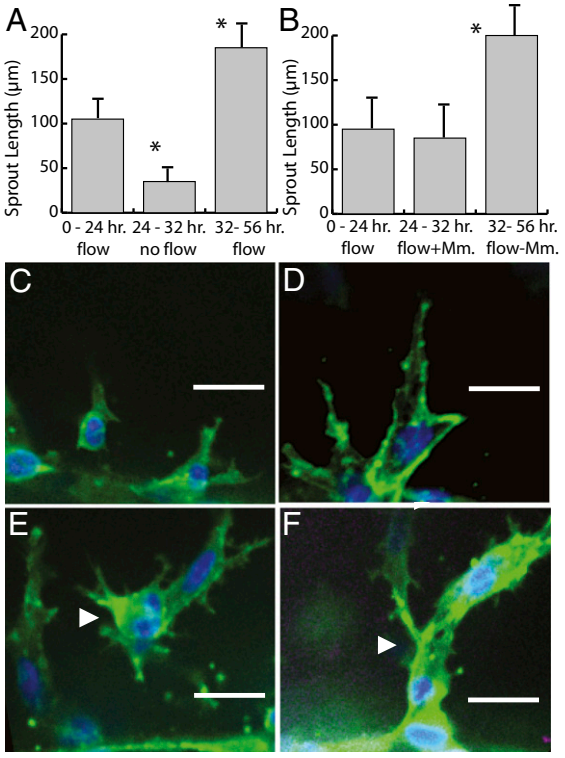

Fig. 3. (*A* and *B*) Mean sprout length after stopping and restarting fluid flow (*A*) and temporary Mamaristat treatment (*B*). Two-sample *t* tests were calculated to determine a significant change from the initial 24-h sprouting response (*P < 0.05). (*C* and *D*) Representative image of sprouts after 8 h of static conditions (*C*) or Mamaristat treatment (*D*). Green, F-actin; blue, nucleus. (Scale bar, 50 μm.) (*E* and *F*) Representative image of sprouts after the 24-h period following resumption of flow (*E*) or washing out of Mamaristat (*F*). White arrowheads point to one of the single-cell sprouts observed in the halted-flow group (*E*) and to the multicellular structures observed in the continuous-flow group (*F*). Green, F-actin; blue, nucleus. (Scale bar, 50 μm.)

Transmural Flow Is Required to Sustain Sprouts. Having established the role of shear stress in inducing endothelial cells to sprout from a monolayer, we next examined whether flow is necessary to sustain a sprout after it has already initiated. We therefore applied transmural flow to cells for 24 h at a flow rate resulting in 11 dyn/cm^2 of shear stress, a quantity known to induce sprouting. After quantifying sprout length, we halted the flow for 8 h. We observed a significant retraction of the sprouts (Fig. 3 *A* and *C*). After restarting flow for an additional 24 h, the sprouts recovered and continued to grow. Because we identified MMP1 as the downstream effector of transmural shear stress, we sought to determine whether blocking MMP activity could produce the same dynamic response as the stop/restart response. After applying 11 dyn/cm^2 of transmural shear stress for 24 h, we added Mamaristat to the perfusing medium for 8 h. Unlike the flow-stop response, Mamaristat simply prevented further extension of sprouts without apparent retraction (Fig. 3 *B* and *D*). After washing out the inhibitor, application of transmural flow for an additional 24 h rescued continued extension.

Confocal microscopy indicated that the structure of the dynamic sprouting response also differed between changes in flow vs. MMP inhibition. Following resumption of flow, endothelial cells recommenced sprouting into the collagen gel, as shown in Fig. 3 *A* and *E*, but mostly as single cells or sprouts containing only two cells (Fig. 3*E*). In contrast, after washing the Mamaristat from the system, the endothelial cells also continued to sprout but did so in the same classical multicellular structures as observed in control sprouts (Fig. 3 *B* and *F*). This result indicates that the action of stopping and resuming fluid flow disrupted the coordinated migration of endothelial cells required to form a multicellular sprout. Interestingly, at the end of both protocols (stop/restart flow, transient Mamaristat treatment), the final mean sprout lengths at 56 h were not significantly different from each other or from those of sprouts under uninterrupted flow (Fig. 3 *A* and *B*). This implies that the rate of sprouting following resumption of flow was greater than the rate during the initial 24 h of transmural flow application. Overall, these results suggest that shear stress from fluid flow not only induces endothelial sprouting but also sustains the sprout and prevents retraction.

Three-Dimensional Focusing of Transmural and Luminal Flows Causes Directed Sprouting. Because one can engineer spatially focused patterns of flow and shear, we explored whether shear-induced sprouting can drive spatial patterns of sprouting. To focus transmural flow, we generated closed-ended voids on opposing sides of a collagen gel such that flow would follow the shortest path across the gel, entering the closed-end, cell-seeded channel, and exit through the wall closest to an acellular void. We constructed finite-element models to predict the fluid shear stress distributions for the different configurations. Fig. 4*A* shows the resulting shear stress distribution of one geometry: two acellular voids placed opposite the cell-seeded void, focusing flow on two corners of the void. Cells were seeded in this geometry and subjected to transmural flow for 48 h. The computational model verified that transmural shear stress exceeded luminal shear stress by approximately two orders of magnitude (Fig. S5). Sprouting appeared to track along the predicted regions of highest transmural shear (Fig. 4*D*) symmetrically along the two corners of the void. Because the frequency of sprouting is somewhat limited, we stacked multiple images of different constructs into a single plot (Fig. 4*G*), showing the increased frequency of sprouting at both corners symmetrically in response to fluid flow. To further illustrate this effect, we generated a second geometry in which only one acellular void is placed opposite the cell-seeded void, such that the transmural flow is focused asymmetrically at only one corner, and the inlet velocity was tuned so that the peak shear stress matched that of the first configuration (Fig. 4*B*). As before, experimental measurements of endothelial sprouting in this configuration again matched the flow profile, in which the highest sprouting frequency was skewed to the corner adjacent to the acellular void (Fig. 4*E*). Stacking multiple images of different constructs again demonstrated the increased frequency of sprouting at the corner adjacent to the void (Fig. 4*H*).

We were also able to spatially pattern the magnitude of luminal flow, by using a channel with a progressively decreasing

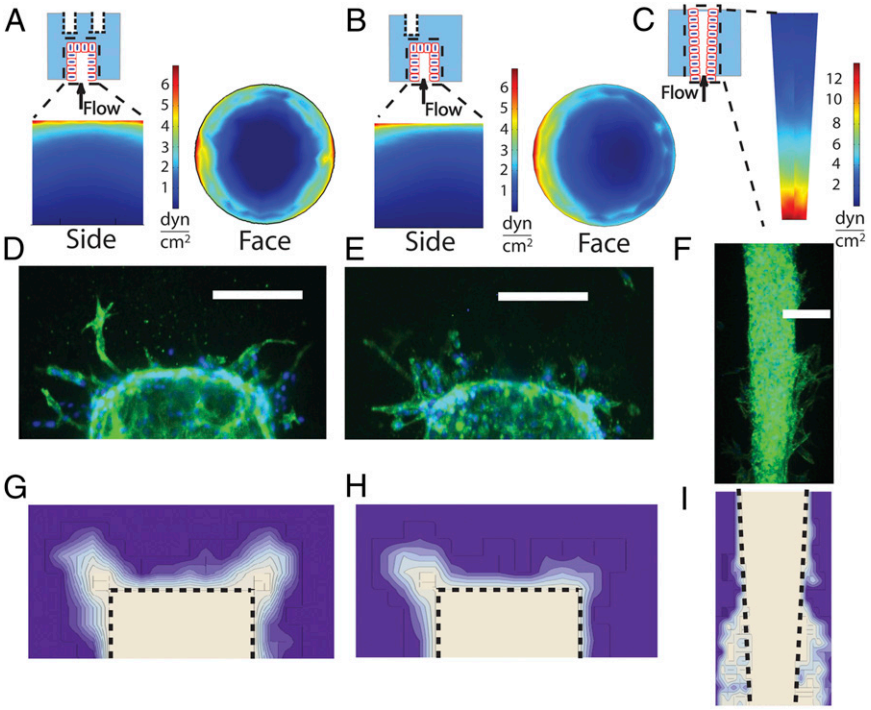

Fig. 4. (*A–C*) Finite-element model predictions of shear stress for the two-void, transmural flow configuration (*A*), the single-void configuration (*B*), and the endothelial-lined nozzle (*C*). (*D–F*) Representative images of the flow-induced sprouting for the three configurations: two-void (*D*), single-void (*E*), and nozzle (*F*). Green, F-actin; blue, nucleus. (Scale bar, 200 μm.) (*G–I*) Frequency plots generated by at least five images of sprouting in the three configurations: two-void (*G*), single-void (*H*), and nozzle (*I*).

radius (henceforth referred to as a "nozzle"). In this configuration, shear stress changes continuously as a function of the radius, allowing for focusing of luminal shear at certain regions of the nozzle surface. The finite-element model indicated that luminal shear stress exceeded unintended transmural shear stress by about an order of magnitude (Fig. S5). Fig. 4*C* shows the shear stress exerted by luminal flow within the nozzle. We used an input flow rate that resulted in the shear threshold occurring approximately midlength of the nozzle. The images and resulting contour plot (Fig. 4 *F* and *I*) show that the frequency of sprouting was substantially increased once the shear stress threshold was surpassed within the nozzle. These results have important implications for flow-induced sprouting in vivo, in addition to verifying the existence of a shear stress threshold, using a different geometry.

Discussion

This study reveals the existence of a shear stress threshold above which sprouting is induced. This threshold response occurs regardless of whether the flow is transmural or luminal, in apparent contrast to previous studies that have reported enhanced sprouting with transmural flow (9–11, 22, 23), but reduced sprouting with luminal shear (9, 24). It is now clear that the reason for the distinct responses was that transmural shears were high whereas the luminal shear used was low. Given that we observed sprouting whether the shear was applied across the apical surface or at cell–cell junctions, it is not surprising that junctional proteins such as VE-cadherin do not participate in transducing the shear stress into the sprouting response, beyond impacting the width between cells through which shear is generated. Although this shear-induced sprouting shares some superficial similarities to the luminal shear stress-induced alignment response of endothelial cells, in that both involve transduction of shears into cytoskeletal reorganization, luminal shear transduction requires a VE-cadherin–containing complex (17, 25). Interstitial flows around single cells embedded within matrices also trigger directed migration, but in such settings, shear stresses as low as 0.1 dyn/cm^2, two orders of magnitude below our reported threshold, are sufficient to drive the response (26–29). Taken together, these studies suggest the conservation of a fundamental link whereby cell movement is stimulated by flow, although the detailed triggers and mechanisms have diverged for different situations.

The mechanisms by which shear stress induces sprouting are likely multifaceted. Here we show that shear stress above the 10 dyn/cm^2 threshold specifically up-regulates the expression of MMP1 but not that of other MMPs. Interestingly, interstitial flow has been reported to up-regulate MMP1 also in migrating smooth muscle cells (30, 31), although several previous reports have shown that shear stress decreases expression of MMP2 and MT1-MMP (32–35). Again, this disparity may result from differences in the levels of shear stress applied to cells or the context in which they have been applied. Nonetheless, the MMP1 response we observed in our studies is clearly relevant, as the up-regulated MMP1 was necessary for shear-induced sprouting. Although it is possible that MMP1 expression is also sufficient to drive sprouting, it is more likely that the development of the complex cytoskeletal structures that give rise to directed invasion is independently triggered by shear stress, and sprouting occurs through the coordination of both processes, matrix degradation and cellular invasion. What remains unclear is how the cytoskeletal processes are regulated and what the molecular basis is for the sharp threshold-like response to shear stress.

The localized concentration of sprouts in different flow patterns reveals the potential significance of this shear-induced response. Our computational model revealed that transmural flow into underlying matrix is highest along the shortest paths (corresponding to least resistance) between a source channel (artery) and a sink channel (lymphatic or venous drain), providing a mechanism for how vessels could sprout along low paths of flow resistance to bridge previously unconnected vessels. For luminal flow, our results suggest that endothelial cells sprout once a threshold of wall shear is surpassed. Thus, if the metabolic needs of a tissue increase, then blood flow is redirected to the area, resulting in enhanced shear stress from both luminal and transmural flows, which in turn triggers endothelial cells to sprout, create collaterals, and reduce the shear stress. Our results also predict that if flow to a certain region is reduced, then the sprouting vessels would prune and retract, also consistent with what occurs in vivo (36). Although this mechanism provides the basic structure for regulating vessel densities in tissue, the presence of other cell types, matrices, and soluble factors in different settings likely can modulate these effects, as exemplified by the effects of low serum on the shear stress threshold reported here. Taken together, these results demonstrate the dynamic and complex interplay between mechanical, geometric, and biochemical factors that endothelial cells use to regulate the remodeling of vascular architecture.

Materials and Methods

The device used in this study consists of a bilayer polydimethylsiloxane (PDMS) mold adhered to a glass coverslip and perfused with a linear syringe pump. Bovine collagen is polymerized within the device, and 400-μm needles are used to create voids in the hydrogel where necessary. Endothelial cells are seeded on the surface of the gel or within the voids, allowed to attach for 30 min or 36 h, and then perfused with flow rates determined from the finite-element simulation used to model the system. Detailed explanations of the materials and methods can be found in *SI Materials and Methods*.

ACKNOWLEDGMENTS. We thank Lin Gao, Dewight Williams, and Ray Meade for technical assistance and Christopher Yu, Evangelia Bellas, Mike Yang, Sarah Stapleton, Jeroen Eyckmans, and Anant Chopra for helpful discussions. This work was supported in part by National Institutes of Health Grants EB00262, EB08396, and EB017103 and the Penn Center for Engineering Cells and Regeneration. P.A.G. acknowledges postdoctoral fellowship support from Grant HL007954.

1. Tuder RM, Flook BE, Voelkel NF (1995) Increased gene expression for VEGF and the VEGF receptors KDR/Flk and Flt in lungs exposed to acute or to chronic hypoxia. Modulation of gene expression by nitric oxide. *J Clin Invest* 95(4):1798–1807.
2. Potente M, Gerhardt H, Carmeliet P (2011) Basic and therapeutic aspects of angiogenesis. *Cell* 146(6):873–887.
3. Kuo L, Davis MJ, Chilian WM (1990) Endothelium-dependent, flow-induced dilation of isolated coronary arterioles. *Am J Physiol* 259(4 Pt 2):H1063–H1070.
4. Dawson JM, Hudlická O (1989) The effects of long term administration of prazosin on the microcirculation in skeletal muscles. *Cardiovasc Res* 23(11):913–920.
5. Egginton S, Zhou AL, Brown MD, Hudlická O (2001) Unorthodox angiogenesis in skeletal muscle. *Cardiovasc Res* 49(3):634–646.
6. Colgan OC, et al. (2007) Regulation of bovine brain microvascular endothelial tight junction assembly and barrier function by laminar shear stress. *Am J Physiol Heart Circ Physiol* 292(6):H3190–H3197.
7. Tarbell JM (2010) Shear stress and the endothelial transport barrier. *Cardiovasc Res* 87(2):320–330.
8. Price GM, et al. (2010) Effect of mechanical factors on the function of engineered human blood microvessels in microfluidic collagen gels. *Biomaterials* 31(24): 6182–6189.
9. Song JW, Munn LL (2011) Fluid forces control endothelial sprouting. *Proc Natl Acad Sci USA* 108(37):15342–15347.
10. Hernández Vera R, et al. (2009) Interstitial fluid flow intensity modulates endothelial sprouting in restricted Src-activated cell clusters during capillary morphogenesis. *Tissue Eng Part A* 15(1):175–185.
11. Semino CE, Kamm RD, Lauffenburger DA (2006) Autocrine EGF receptor activation mediates endothelial cell migration and vascular morphogenesis induced by VEGF under interstitial flow. *Exp Cell Res* 312(3):289–298.
12. Tarbell JM, Weinbaum S, Kamm RD (2005) Cellular fluid mechanics and mechanotransduction. *Ann Biomed Eng* 33(12):1719–1723.
13. Tarbell JM, Demaio L, Zaw MM (1999) Effect of pressure on hydraulic conductivity of endothelial monolayers: Role of endothelial cleft shear stress. *J Appl Physiol (1985)* 87(1):261–268.
14. Parker JC, Stevens T, Randall J, Weber DS, King JA (2006) Hydraulic conductance of pulmonary microvascular and macrovascular endothelial cell monolayers. *Am J Physiol Lung Cell Mol Physiol* 291(1):L30–L37.
15. Galie PA, Spilker RL, Stegemann JP (2011) A linear, biphasic model incorporating a brinkman term to describe the mechanics of cell-seeded collagen hydrogels. *Ann Biomed Eng* 39(11):2767–2779.

16. Carmeliet P, et al. (1999) Targeted deficiency or cytosolic truncation of the VE-cadherin gene in mice impairs VEGF-mediated endothelial survival and angiogenesis. *Cell* 98(2):147–157.
17. Tzima E, et al. (2005) A mechanosensory complex that mediates the endothelial cell response to fluid shear stress. *Nature* 437(7057):426–431.
18. Jinga VV, Bogdan I, Fruchter J (1986) Experimental model for the quantitative estimation of transendothelial transport in vitro; a two-compartment system. *Physiologie* 23(4):227–236.
19. Chrobak KM, Potter DR, Tien J (2006) Formation of perfused, functional microvascular tubes in vitro. *Microvasc Res* 71(3):185–196.
20. Partridge CR, Hawker JR, Jr., Forough R (2000) Overexpression of a secretory form of FGF-1 promotes MMP-1-mediated endothelial cell migration. *J Cell Biochem* 78(3):487–499.
21. Nguyen DH, et al. (2013) Biomimetic model to reconstitute angiogenic sprouting morphogenesis in vitro. *Proc Natl Acad Sci USA* 110(17):6712–6717.
22. Kang H, Bayless KJ, Kaunas R (2008) Fluid shear stress modulates endothelial cell invasion into three-dimensional collagen matrices. *Am J Physiol Heart Circ Physiol* 295(5):H2087–H2097.
23. Kang H, Kwak HI, Kaunas R, Bayless KJ (2011) Fluid shear stress and sphingosine 1-phosphate activate calpain to promote membrane type 1 matrix metalloproteinase (MT1-MMP) membrane translocation and endothelial invasion into three-dimensional collagen matrices. *J Biol Chem* 286(49):42017–42026.
24. Chouinard-Pelletier G, Jahnsen ED, Jones EA (2013) Increased shear stress inhibits angiogenesis in veins and not arteries during vascular development. *Angiogenesis* 16(1):71–83.
25. Yamamoto K, et al. (2005) Fluid shear stress induces differentiation of Flk-1-positive embryonic stem cells into vascular endothelial cells in vitro. *Am J Physiol Heart Circ Physiol* 288(4):H1915–H1924.
26. Wang DM, Tarbell JM (1995) Modeling interstitial flow in an artery wall allows estimation of wall shear stress on smooth muscle cells. *J Biomech Eng* 117(3): 358–363.
27. Galie PA, Russell MW, Westfall MV, Stegemann JP (2012) Interstitial fluid flow and cyclic strain differentially regulate cardiac fibroblast activation via AT1R and TGF-β1. *Exp Cell Res* 318(1):75–84.
28. Ng CP, Hinz B, Swartz MA (2005) Interstitial fluid flow induces myofibroblast differentiation and collagen alignment in vitro. *J Cell Sci* 118(Pt 20):4731–4739.
29. Polacheck WJ, Charest JL, Kamm RD (2011) Interstitial flow influences direction of tumor cell migration through competing mechanisms. *Proc Natl Acad Sci USA* 108(27): 11115–11120.
30. Shi ZD, Ji XY, Qazi H, Tarbell JM (2009) Interstitial flow promotes vascular fibroblast, myofibroblast, and smooth muscle cell motility in 3-D collagen I via upregulation of MMP-1. *Am J Physiol Heart Circ Physiol* 297(4):H1225–H1234.
31. Shi ZD, Ji XY, Berardi DE, Qazi H, Tarbell JM (2010) Interstitial flow induces MMP-1 expression and vascular SMC migration in collagen I gels via an ERK1/2-dependent and c-Jun-mediated mechanism. *Am J Physiol Heart Circ Physiol* 298(1):H127–H135.
32. Milkiewicz M, Kelland C, Colgan S, Haas TL (2006) Nitric oxide and p38 MAP kinase mediate shear stress-dependent inhibition of MMP-2 production in microvascular endothelial cells. *J Cell Physiol* 208(1):229–237.
33. Rivilis I, et al. (2002) Differential involvement of MMP-2 and VEGF during muscle stretch- versus shear stress-induced angiogenesis. *Am J Physiol Heart Circ Physiol* 283(4):H1430–H1438.
34. Sho E, et al. (2002) Arterial enlargement in response to high flow requires early expression of matrix metalloproteinases to degrade *extracellular matrix*. *Exp Mol Pathol* 73(2):142–153.
35. Yun S, et al. (2002) Transcription factor Sp1 phosphorylation induced by shear stress inhibits membrane type 1-matrix metalloproteinase expression in endothelium. *J Biol Chem* 277(38):34808–34814.
36. Isogai S, Lawson ND, Torrealday S, Horiguchi M, Weinstein BM (2003) Angiogenic network formation in the developing vertebrate trunk. *Development* 130:5281–5290.

Supporting Information

Galie et al. 10.1073/pnas.1310842111

SI Materials and Methods

Microfabrication. SU-8 photoresist was deposited on a silicon wafer and patterned using traditional photolithography. The resulting master was then used to create polydimethylsiloxane (PDMS) devices with a central chamber in which collagen could be polymerized. The PDMS was treated with 10 N sulfuric acid to etch the surface followed by incubation with dilute collagen to facilitate collagen gel attachment. This attachment method prevented gel compaction of the 2-mg/mL collagen gel during the flow experiments. The permeability of the collagen was $5.4E\text{-}14$ m^2, a value measured by Galie et al. in a previously published paper (1). To create the luminal configuration and 3D void networks, blunted stainless steel needles were placed within the collagen before polymerization. For the nozzle design, a glass pipette was pulled to create the decreasing diameter and treated with 0.2% pluronic before use.

Cell Culture and Seeding. All experiments were performed using passage 7 HUVECs (Lonza) 3–5 d after thawing and feeding with endothelial cell growth media (EGM-2). Cells were injected into the device to create a uniform seeding density of 10,000 cells/cm^2. Thirty-six hours after seeding the cells into the device, a syringe pump was attached to the PDMS device to deliver fluid flow. For the 2D studies, flow was applied for 20–24 h. For the 3D studies, flow was applied for 42–48 h. Sprout lengths were measured by finding the distance between the monolayer and the tip of the invading cell, using bright-field images imported into ImageJ software.

Confocal Microscopy. After fixing with 3.7% (wt/vol) paraformaldehyde and permeabilization of the membrane with Triton X-100, cells were stained with phalloidin conjugated to Texas Red, DAPI, β-catenin, or 1-μm beads labeled with FITC. A spinning-disk confocal microscope was used to image the monolayers at 63× and the sprouting 3D configurations at 10× and 20×. For the monolayer images, PBS containing the 1-μm beads was flowed normal to the surface of the monolayer after the completion of the experiment, but before fixing.

Quantitative RT-PCR. mRNA was isolated from cells by solubilization with TRIzol buffer combined with ethanol and run through an RNeasy minikit. A DNase step was used during the RNA purification process. Reverse transcription was performed using a qScript cDNA kit. Primers for GAPDH, matrix metalloproteinase 1 (MMP1), MMP2, MMP9, MMP10, and MMP14 (IDT) were used to amplify cDNA. Double normalization was performed by comparing amplification of the primers to that of GAPDH and static control.

MMP1 mRNA Silencing. Dicer substrate interference RNA (DsiRNA) against MMP1 mRNA (IDT) was transfected into the cells, using Lipofectamine per the manufacturer's protocol. DsiRNA was added to the cells before washing after an overnight incubation. Cells were then fed with normal EGM-2 for one full day before use in experiments.

VEΔ Adenovirus. An adenovirus containing the VEΔ or GFP control construct (previously described in ref. 2) was added to HUVECs and incubated overnight. The virus was titrated to maximize the number of cells expressing GFP while minimizing cell death. After washing, the cells were cultured for 2 d before use in experiments.

Finite-Element Modeling. COMSOL software was used to generate the computational models used in this study. For all models, the hydraulic conductivity of the endothelial monolayers was used to describe fluid mechanics of the system. A Stokes flow governing equation was used to describe all nonporous flow, whereas a Brinkman equation was used to describe the flow through the collagen hydrogel. At the nonporous and porous boundaries, a velocity-matching boundary condition was used. Inlet boundary conditions were used to match the applied flow of the syringe pumps, and outlet boundary conditions were 0 Pa because all flows exited into atmosphere. See Figs. S4 and S5 for detailed boundary conditions.

Atomic Force Microscopy. We used a pyramid tip silicon nitride probe in tapping mode to measure the topography of 50 × 50-μm sections of the monolayer after exposure to fluid flow. Resulting surface plots were then quantified to determine the height profile of the monolayer, focusing specifically on the gaps formed in monolayers exposed to transmural flow.

Transmission Electron Microscopy. Samples were fixed in a solution containing 4% formaldehyde and 2.5% glutaraldehyde, before preparation for transmission electron microscopy (TEM). Transverse sections of the collagen gel with endothelial cells spread on the surface are cut into thin sections, embedded, and placed in an EM grid for visualization.

Transmural Shear Stress Calculation

Flow in the Junction Is Laminar and Fully Developed for Both Mature and Immature Monolayers. The Reynolds number (Re) can be calculated from the cell–cell junction geometry and velocity of the flow. The velocity of flow through the junctions can be calculated using an equation from Tarbell et al. (3), which represents conservation of mass for an incompressible fluid,

$$\overline{V} = J_V \frac{A}{Pd}, \qquad \text{[S1]}$$

where J_V is velocity of fluid normal to the monolayer, A is the total cross-sectional area of the monolayer, P is the total perimeter of cells, and d is the junctional distance. For a mature monolayer exposed to a superficial velocity of 10 nm/s, the junctional velocity is 11 μm/s. For an immature monolayer exposed to a superficial velocity of 10 μm/s, the junctional velocity is 0.25 mm/s. Hence, the Re of flow within the junction for both mature and immature monolayers is

$$\mathrm{Re} = \frac{\rho \overline{V} d}{\mu} << 1. \qquad \text{[S2]}$$

Because the flow is clearly laminar, the entrance length of the flow can be estimated using a relationship for parallel plates (4):

$$L_e = \left(\frac{0.315}{0.0175\ \mathrm{Re} + 1} + 0.011\ \mathrm{Re} \right) d. \qquad \text{[S3]}$$

Because Re << 1 within the cell junctions, the entrance length can be approximated as $0.315d$. We used our finite-element model to numerically simulate flow through parallel plates with dimensions identical to the measured junction geometries and found similar entrance lengths (defining entrance length as the distance required for the centerline velocity to reach 99% of its

fully developed value). For the mature junctions, the longest entrance length occurs in the VEΔ-treated cells: 22.85 nm or 1.87% of the junction length. For immature junctions, the entrance length is considerably longer at 139.86 nm or 12.95% of the junction length. Hence, even for the longest entrance length, the junction is still fully developed for over 87% of its length. Hence, we believe the fully developed assumption is valid for our calculations.

Mature Junctions Are Idealized as Continuous Parallel Plates. Because the flow is laminar and fully developed, the Stokes equation is sufficient to solve the flow. The geometry of the junctions is idealized as continuous parallel plates (Fig. S2) so that the resistance to fluid flow (ratio of pressure drop to volumetric flow rate) is

$$R_{\text{cells}} = \frac{3\mu L_j}{2p(d/2)^3}, \quad \text{[S4]}$$

where L_j is the mean length of the junctions, d is the width of the junctions, and p is the total perimeter of cells forming the monolayer. These parameters are measured using a combination of transmission electron microscopy and fluorescence microscopy (*Parameter Estimation* section).

Calculating the Resistances of the Parallel Circuit Used for Mature Monolayers. To achieve superficial velocities on the order of nanometers per second within the microscale device, flow is pushed through a parallel circuit: One device contains only a 2-mg/mL collagen gel with a permeability of 5.4*E*-14 m^2, as determined by a previous study (1), and the other device contains cells plated on the collagen and incubated for 36 h. The resistance to fluid flow provided by the acellular gel is calculated from Darcy's law,

$$R_{\text{collagen}} = \frac{\mu L_c}{kA}, \quad \text{[S5]}$$

where L_c is the length of the collagen gel, k is the permeability, and A is the cross-sectional area.

The total resistance of the parallel circuit is then

$$R_T^{-1} = \frac{1}{R_{\text{cells}} + R_{\text{collagen}}} + \frac{1}{R_{\text{collagen}}}. \quad \text{[S6]}$$

Using a parallel circuit of a known resistance, the superficial velocity delivered to the cell-seeded gel can be appropriately reduced.

Shear Stress Can Be Calculated from Pressure Drop and Geometry for the Mature Monolayers. To determine the pressure drop across the monolayer for a given volumetric flow rate, Q, the total resistance of the parallel circuit is calculated and used in the following equation:

$$\Delta P = R_T Q. \quad \text{[S7]}$$

Again, because the flow is modeled as Stokes flow in idealized geometries, the shear stress on the walls of the junctions is directly proportional to the pressure:

$$\tau = \frac{\Delta P d}{2L_j}. \quad \text{[S8]}$$

Immature Junctions Are Idealized as Parallel Plates and the Nonconfluent Gaps Between Cells Are Modeled as Cylinders. Because the flow is laminar and fully developed, the Stokes equation is sufficient to solve the flow. The geometry of the cell–cell junctions is idealized as continuous parallel plates and the gaps are idealized as discrete cylinders, respectively. Therefore, their resistance to fluid flow (ratio of pressure drop to volumetric flow rate) can be shown to be

$$R_j = \frac{3\mu L_j}{2p(d/2)^3} \quad \text{[S9]}$$

$$R_g = \frac{8\mu L_g}{\pi r^4}, \quad \text{[S10]}$$

where L is the length or height of the cell–cell junction/gap.

Resistances of Immature Junctions and Gaps Are Added in Parallel. To determine the pressure drop across the monolayer for a given volumetric flow rate, Q, the resistance from the junctions (one entity) is added in parallel with the resistance of the individual gaps.

$$\Delta P = R_T Q \quad \text{[S11]}$$

$$R_T^{-1} = \frac{1}{R_j + nR_g}, \quad \text{[S12]}$$

where n is the gap multiplier (number of gaps for each monolayer).

Shear Stress Can Be Calculated from Pressure Drop and Geometry for the Immature Monolayers. Again, because the flow is modeled as Stokes flow in idealized geometries, the shear stress on the walls of the cell–cell junctions and gaps can be shown to be

$$\tau_j = \frac{\Delta P d}{2L_j} \quad \text{[S13]}$$

$$\tau_g = \frac{\Delta P d}{2L_g}. \quad \text{[S14]}$$

Shear stress at the cell–cell junctions was found to always exceed the shear at the cell gaps.

Parameter Estimation

Mature Monolayers. ***Total cell perimeter (p).***

Measurement method. Confocal microscopy.

Rationale. Using images taken at 40× of cells labeled for actin and β-catenin, cell perimeters are traced (dotted lines in Figs. S2 and S3) and averaged across several images to generate a ratio of perimeter to area. This number is then multiplied by the total area of the flow device to yield a total perimeter. This process is conducted for control, VEΔ, and low serum test groups and yields (0.0639 ± 0.01785 m, 0.0724 ± 0.02984 m, and 0.0613 ± 0.01424 m, respectively).

Junction size (d, L_j).

Measurement method. TEM, confocal microscopy.

Rationale. Confocal microscopy provides a global view of the junctions between cells, whereas TEM yields a localized snapshot of the junction geometry. The widths of the cell–cell junctions are measured at multiple points along the cell membranes and averaged for control, VEΔ, and low serum test groups (27.98 ± 10.2 nm, 72.54 ± 16.8 nm, and 31.134 ± 11.5 nm, respectively). The lengths are 1.51 ± 0.501, 1.22 ± 0.314, and 1.45 ± 0.423 μm, respectively.

Immature Monolayers. ***Total cell perimeter (p).*** Using images taken at 40× of cells labeled for actin and β-catenin, cell perimeters are traced (dotted lines in Figs. S2 and S3) and averaged across several

images to generate a mean ratio of perimeter to area. This number is then multiplied by the total area of the flow device to yield a total perimeter. This process yields $P = 0.0446 \pm 0.0092$ m.

Gap radius/height (r, L_g). For control cells exposed to transmural flow, large (~10 μm) gaps exist in the monolayer. To determine the geometry of these gaps, confocal microscopy is used to visualize the accumulation of 2-μm beads in these spaces, although these images are not used for the estimation of gap geometry. The presence of the gaps is also verified by TEM measurements. However, AFM conducted with a pyramid tip provides a quantitative measure of the radius and height of the gap. The average gap radius is calculated to be $r = 4.54 \pm 0.94$ μm, and the average height $L_g = 6.79 \pm 2.98$ μm.

Gap multiplier (n). To determine the number of gaps across the entire monolayer, the fluorescent beads flowed normal to the surface are visualized with low-magnification microscopy. The number of bead accumulations is added for multiple images and averaged over the entire surface of the monolayer ($n = 181 \pm 28$ gaps).

Junction size (d, L_j). Confocal microscopy provides a global view of the cell–cell junctions, whereas TEM yields a localized snapshot of the geometry. Only TEM measurements are used to calculate the parameters d (junction width) and L_j (junction length). For control cells, the cell–cell junctions are interdigitated and remain less than 100 nm apart along the length of the junction. However, for cells exposed to flow, there are sections of the cell–cell junction with larger openings. For each junction the width is averaged along several points of the length of the junction. This is repeated for three junctions to estimate a mean width ($d = 444 \pm 104$ nm) for the control group. The mean height of the junctions is $L_j = 1.08 \pm 0.192$.

Error Analysis. Because small deviations in these estimated parameters can have a major impact on the shear stress calculations, the SDs in these measurements must be propagated to the error in the calculated stress. The following formula is used to implement this error propagation:

$$s_\tau = \sqrt{\left(\frac{\partial \tau}{\partial p}\right)^2 s_p + \left(\frac{\partial \tau}{\partial d}\right)^2 s_d + \left(\frac{\partial \tau}{\partial L}\right)^2 s_L}. \qquad \text{[S15]}$$

Similarly, the volumetric flow passing through the cell-seeded device can also be calculated using these parameters. As a validation of the assumptions used to calculate junctional velocity, pressure drop, and shear stress, the volume of fluid pumped through the cell-seeded device was compared with the calculated range of flow rates and found to be within 1 SD of the predicted rate.

Entrance Length Supplement

Calculations of transmural shear stress are performed in the study assuming that flow within the cell–cell junctions is fully developed. However, flow within any channel requires a finite length to develop; this region is referred to as the entrance length. Because Re <<1, the above equation suggests that the ratio of entrance length to channel diameter = 0.315. Thus, depending on the geometry of the channels, the entrance length can be a sizeable fraction of the total length of the channel. The table below summarizes the average geometries of the channels determined from TEM measurements and uses the Shah and London equation (4) to estimate what percentage of the total length is required to fully develop the flow profile.

Sample	Treatment	Junction length, nm	Junction width, nm	Entrance length, nm	Fraction of total length
1	Mature control	1,510	27.98	8.814	0.0058
2	Mature VEΔ	1,220	72.54	22.85	0.0187
3	Mature low serum	1,450	31.134	9.807	0.0068
4	Immature	1,080	444	139.86	0.129

As the table indicates, the mature monolayers all exhibit an entrance length less than 2% of the total length. However, for the immature monolayer, the entrance length is ~13% of the total length. Because shear stress is increased along the entrance length, we must quantify how much the developing flow augments shear stress to validate the fully developed assumption.

The table below summarizes the effect of accounting for the entrance length in the four channel geometries in our finite-element model.

Sample	Treatment	% increase in shear
1	Mature control	0.21
2	Mature VEΔ	0.78
3	Mature low serum	0.34
4	Immature	3.8

The finite-element model estimates that, even for the immature monolayer, the entrance length is responsible for less than a 4% increase in shear compared with values calculated assuming fully developed flow.

A possible explanation for the diminutive increase in shear stress is the parabolic shape of the velocity distribution at the channel inlet. Shear stress is elevated along the entrance length because friction is required to slow flow near the wall to create a fully developed, parabolic velocity profile. The more uniform that an inlet velocity profile is, the more friction (and shear stress) is required to develop the flow. However, for our geometries, the flow has a parabolic shape even before the inlet because of funneling into the cell–cell junctions. Moreover, the no-slip condition at the wall combined with the low Re of the flow creates additional nonuniformity in the velocity distribution at the inlet, further reducing the friction required to fully develop the flow. To illustrate this effect below, arrows representing x and y velocity components of flow entering immature junctions are overlaid on a pressure contour:

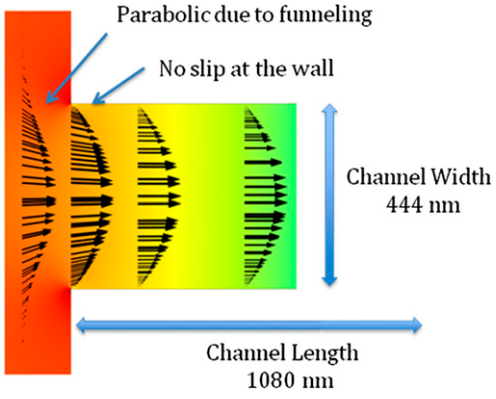

1. Galie PA, Spilker RL, Stegemann JP (2011) A linear, biphasic model incorporating a brinkman term to describe the mechanics of cell-seeded collagen hydrogels. *Ann Biomed Eng* 39(11):2767–2779.

2. Nelson CM, Pirone DM, Tan JL, Chen CS (2004) Vascular endothelial-cadherin regulates cytoskeletal tension, cell spreading, and focal adhesions by stimulating RhoA. *Mol Biol Cell* 15(6):2943–2953.

3. Tarbell JM, Demaio L, Zaw MM (1999) Effect of pressure on hydraulic conductivity of endothelial monolayers: Role of endothelial cleft shear stress. *J Appl Physiol (1985)* 87(1):261–268.

4. Shah RK, London AL (1978) *Laminar Flow Forced Convection in Ducts*, Advances in Heat Transfer, Suppl 1 (Academic, New York).

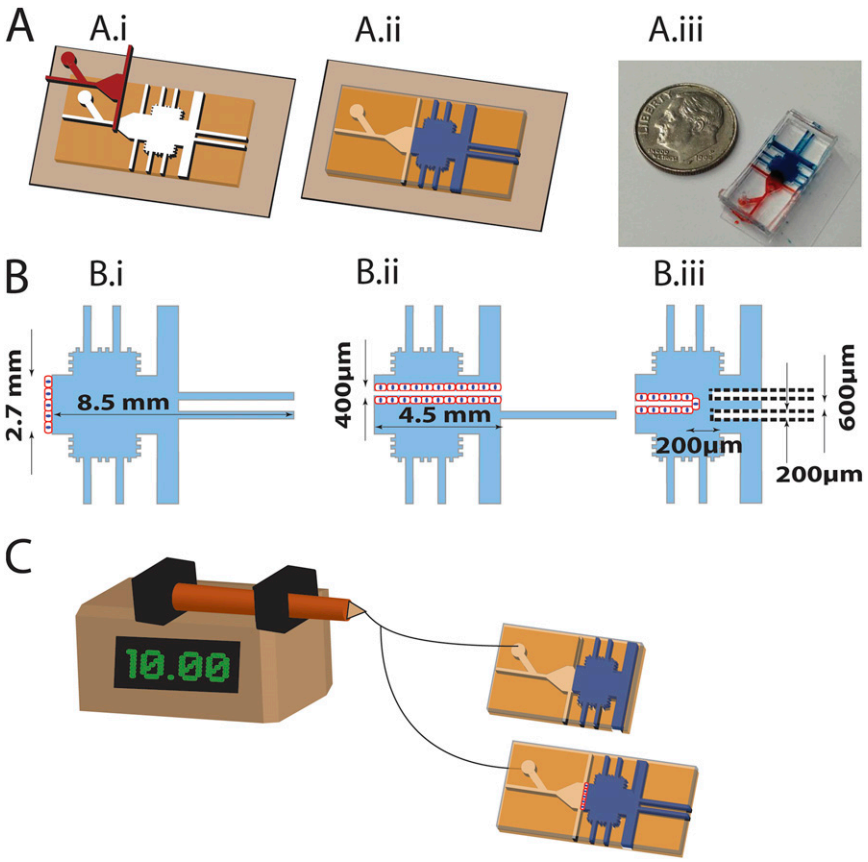

Fig. S1. (*A*) The device is prepared by plasma etching the PDMS surface with an insert (red) in place to create a hydrophobic/hydrophilic barrier to control the placement of the acid etch (*A*, *i*), so that the collagen hydrogel (blue) is constrained only to the central chamber of the device (*A*, *ii*). Food coloring is used to highlight the resulting positioning of the collagen hydrogel (*A*, *iii*). (*B*) The device is used in three configurations: a plug configuration for the transmural flow experiments (*B*, *i*), a flow-through cylindrical void for the luminal flow experiments (*B*, *ii*), and closed-end cylindrical voids for the directed sprouting assays (*B*, *iii*). (*C*) Flow is applied in a parallel circuit to achieve low (on the scale of nanoliters per minute)-magnitude flows. An acellular gel of known permeability is used as the secondary circuit, and estimations of the hydraulic conductivity of the cell monolayer are used to calculate the ratio of flow that passes through the cell-seeded device.

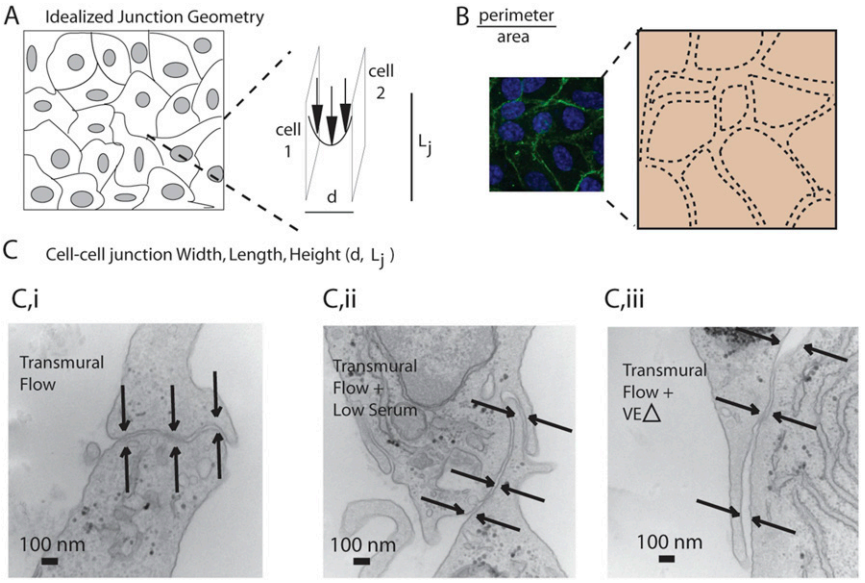

Fig. S2. Schematic of the idealized geometries used to calculate shear stress for a given volumetric flow rate through the endothelial monolayer. (*A*) Cell–cell junctions are idealized as a continuous set of parallel plates. (*B*) Calculation of the perimeter to area ratio, which is required to determine the total perimeter of the cell–cell junctions for the given endothelial monolayer. (*C*) TEM results used to determine the cell–cell junction geometry of transmural flow through untreated (*C*, *i*), low serum (*C*, *ii*), and VEΔ (*C*, *iii*) conditions. These images are representative of the cell–cell junctions for each condition. A mean junction width was calculated by taking several measurements along the length of each junction (represented by the black arrows) and averaging over at least three junctions. The variance is calculated between different junctions. (Scale bar, 100 nm.)

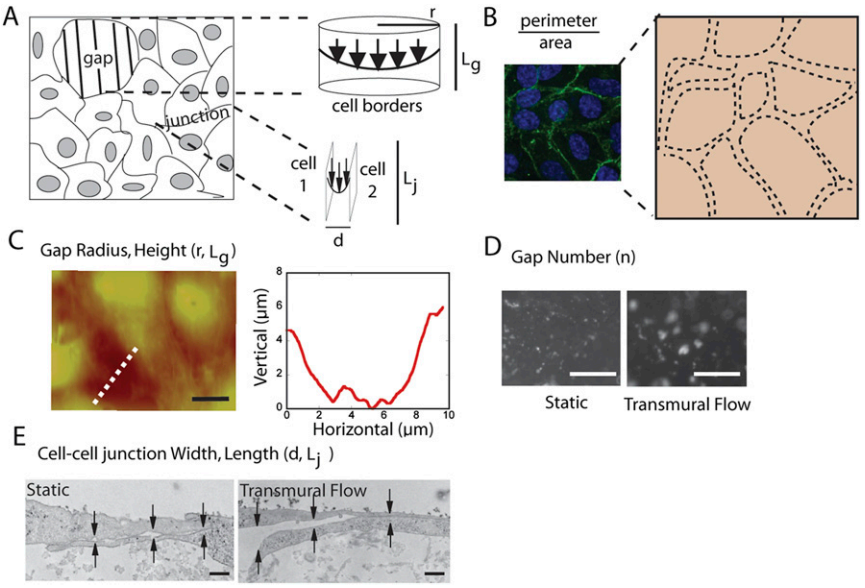

Fig. S3. (*A*) Schematic of the idealized geometries used to calculate shear stress for a given volumetric flow rate through the immature endothelial monolayer. Circular gaps between cells are idealized as cylinders, and cell–cell junctions are idealized as a continuous set of parallel plates. (*B*) Calculation of the perimeter to area ratio, which is required to determine the total perimeter of the cell–cell junctions for the given endothelial monolayer. (*C*) Results of AFM tapping to determine the geometry of the circular gaps in the endothelial monolayer: A topographical map is used to determine the height profile and radius of the gaps. (*D*) Distribution of fluorescent beads flowed against the endothelial monolayer after static and transmural flow conditions. (Scale bars, 30 μm.) (*E*) TEM results used to determine the cell–cell junction geometry of static and transmural flow conditions. These images are representative of the cell–cell junctions for each condition. A mean junction width was calculated by taking several measurements along the length of each junction (represented by the black arrows) and averaging over at least three junctions. The variance is calculated between different junctions. (Scale bars, 1 μm.)

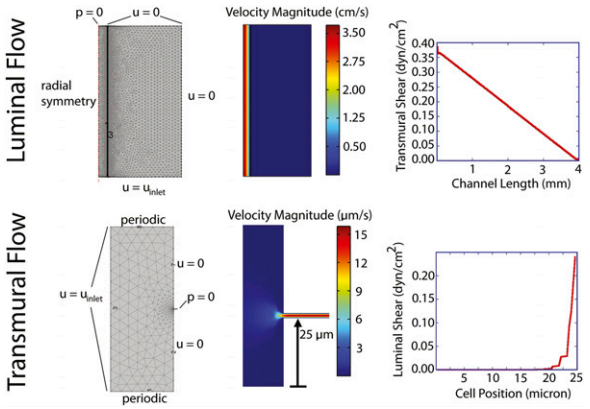

Fig. S4. Two-dimensional finite-element analysis shows that the testing configurations isolate transmural and luminal flows. Boundary conditions and mesh sizes are shown for both predominantly luminal and transmural flow conditions. The elements are formulated to represent free-flowing medium, collagen hydrogel, or the cell monolayer. Fluid and collagen properties are input to describe the flow through these domains, and an artificial permeability is assigned to the monolayer elements to mimic the hydraulic conductivity of the monolayer. Flow through the cell-seeded, cylindrical channel creates a pressure difference across the cell layer, but that pressure drop is substantially less than the axial pressure drop along the length of the channel. For this reason, the peak transmural shear is only 0.4 dyn/cm^2, occurring at the initial position of the channel. Similarly, a simplified model of a cell–cell junction with flow normal to the surface indicates that there is negligible luminal shear during application of transmural flow. The peak luminal shear of 0.248 dyn/cm^2 is localized to the junction. In both cases, when applying transmural or luminal shear on the magnitude of 10 dyn/cm^2, the shear stress produced by the alternate mode of shear is two orders of magnitude less.

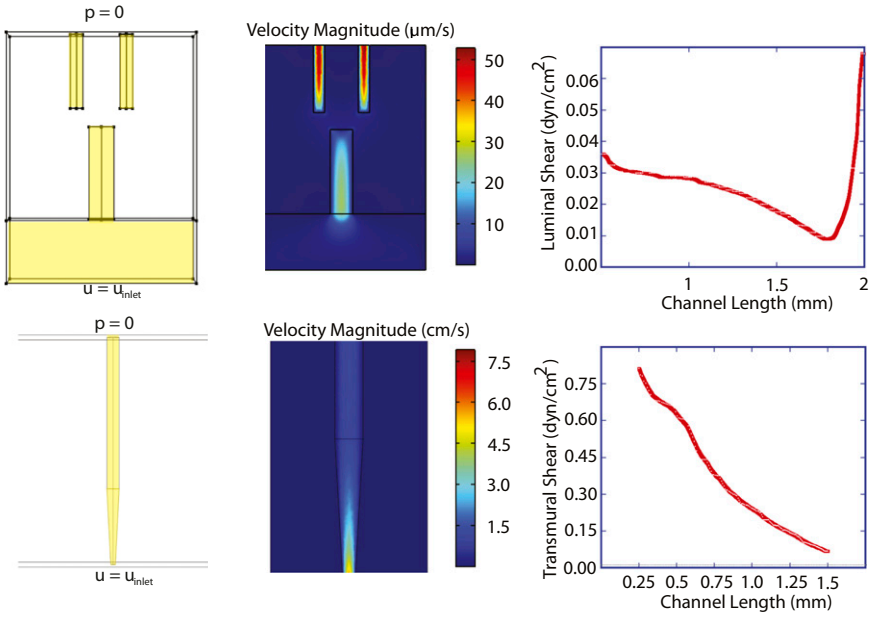

Fig. S5. Three-dimensional finite-element analysis shows that transmural and luminal shears are also isolated in the 3D sprouting assays. The luminal shear along the closed-end channel peaks at the end of the closed channel, at ~0.07 dyn/cm^2. Likewise, transmural flow through the nozzle configuration peaks at 0.74 dyn/cm^2 at the entrance of the nozzle.